NeuroImage 83 (2013) 135–147

Contents lists available at ScienceDirect

NeuroImage

journal homepage: www.elsevier.com/locate/ynimg

Measurement of OEF and absolute $CMRO_2$: MRI-based methods using interleaved and combined hypercapnia and hyperoxia

Richard G. Wise *, Ashley D. Harris, Alan J. Stone, Kevin Murphy

Cardiff University Brain Research Imaging Centre (CUBRIC), School of Psychology, Cardiff University, Park Place, Cardiff CF10 3AT, UK

ARTICLE INFO

Article history:
Accepted 5 June 2013
Available online 13 June 2013

Keywords:
BOLD
$CMRO_2$
CBF
Oxygen metabolism
Hypercapnia
Hyperoxia

ABSTRACT

Blood oxygenation level dependent (BOLD) functional magnetic resonance imaging (fMRI) is most commonly used in a semi-quantitative manner to infer changes in brain activity. Despite the basis of the image contrast lying in the cerebral venous blood oxygenation level, quantification of absolute cerebral metabolic rate of oxygen consumption ($CMRO_2$) has only recently been demonstrated. Here we examine two approaches to the calibration of fMRI signal to measure absolute $CMRO_2$ using hypercapnic and hyperoxic respiratory challenges. The first approach is to apply hypercapnia and hyperoxia separately but interleaved in time and the second is a combined approach in which we apply hyperoxic challenges simultaneously with different levels of hypercapnia. Eleven healthy volunteers were studied at 3 T using a dual gradient-echo spiral readout pulsed arterial spin labelling (ASL) imaging sequence. Respiratory challenges were conducted using an automated system of dynamic end-tidal forcing. A generalised BOLD signal model was applied, within a Bayesian estimation framework, that aims to explain the effects of modulation of CBF and arterial oxygen content to estimate venous deoxyhaemoglobin concentration ($[dHb]_0$). Using CBF measurements combined with the estimated oxygen extraction fraction (OEF), absolute $CMRO_2$ was calculated. The interleaved approach to hypercapnia and hyperoxia, as well as yielding estimates of $CMRO_2$ and OEF demonstrated a significant increase in regional CBF, venous oxygen saturation (SvO_2) (a decrease in OEF) and absolute $CMRO_2$ in visual cortex in response to a continuous (20 min) visual task, demonstrating the potential for the method in measuring long term changes in $CMRO_2$. The combined approach to oxygen and carbon dioxide modulation, as well as taking less time to acquire data, yielded whole brain grey matter estimates of $CMRO_2$ and OEF of 184 ± 45 μmol/100 g/min and 0.42 ± 0.12 respectively, along with additional estimates of the vascular parameters $\alpha = 0.33 \pm 0.06$, the exponent relating relative increases in CBF to CBV, and $\beta = 1.35 \pm 0.13$, the exponent relating deoxyhaemoglobin concentration to the relaxation rate R_2^*. Maps of cerebrovascular and cerebral metabolic parameters were also calculated. We show that combined modulation of oxygen and carbon dioxide can offer an experimentally more efficient approach to estimating OEF and absolute $CMRO_2$ along with the additional vascular parameters that form an important part of the commonly used calibrated fMRI signal model.

Introduction

Blood oxygenation level dependent (BOLD) fMRI is commonly used to map changes in brain activity levels but is normally performed without quantification of the underlying cerebral metabolism. fMRI is widely used as a tool in basic neuroscientific and clinical research as well as being applied clinically in a qualitative manner for pre-surgical functional mapping. Advancing methods that are able to quantify cerebrovascular and cerebral metabolic function would render fMRI considerably more useful in clinical research and clinical application across a wide range of diseases. This process has begun with the improvement in recent years of arterial spin labelling (ASL) methods for measuring cerebral blood flow (CBF). However, until recently, radiotracer techniques such as ^{15}O PET have offered the only means of quantifying absolute cerebral oxygen metabolism. The requirement for radiotracers limits the application of such measurements longitudinally and in healthy volunteers, hampering studies of disease evolution, brain development and ageing.

The predominantly aerobic production of ATP in the healthy brain means that the local cerebral rate of metabolic oxygen consumption ($CMRO_2$) closely parallels neural energy consumption. Therefore, it potentially offers a stable and robust marker of the (patho)physiological state of brain tissue for assessing longitudinal changes in regional brain function with plasticity and learning, neurological and psychiatric diseases, and treatment interventions. An MRI based method for examining relative changes in $CMRO_2$ was introduced in 1998 (Davis et al., 1998). This method, employing a (presumed-isometabolic) hypercapnic vasodilatory stimulus, is restricted to estimating fractional changes in $CMRO_2$ relative to a within-session baseline and over a timescale restricted by the sensitivity to BOLD signal changes, typically a few

* Corresponding author at: CUBRIC, School of Psychology, Cardiff University, Park Place, Cardiff CF10 3AT, UK. Fax: +44 29 208 70339.
E-mail address: wiserg@cardiff.ac.uk (R.G. Wise).

1053-8119/$ – see front matter © 2013 Elsevier Inc. All rights reserved.
http://dx.doi.org/10.1016/j.neuroimage.2013.06.008

seconds to a few minutes. A similar method was proposed for oxygen-based calibration of the BOLD signal by Chiarelli et al. (2007), with the limitation of needing to assume the fraction of oxygen extracted from arterial blood on its passage to the veins (oxygen extraction fraction, OEF). Interpretation of the biological significance of relative changes in $CMRO_2$ is problematic where the baseline $CMRO_2$ may be altered in disease or drug studies (Iannetti and Wise, 2007).

MR methods have begun to emerge for estimating absolute rather than relative $CMRO_2$. Methods yielding bulk or whole brain $CMRO_2$ are based on measurement of CBF and venous oxygen saturation via the T_2 of venous blood (Lu and Ge, 2008; Xu et al., 2009) or the pattern of magnetic field distortions around major veins (Fan et al., 2012). However, the spatial resolution of such methods is restricted to the volume of brain tissue being drained by the vein of interest. Velocity selective methods have also been used to isolate the T_2 of venous blood and estimate its oxygenation based on a T_2-oxygenation calibration curve (Bolar et al., 2011; Guo and Wong, 2012). A quantitative or qBOLD approach has also been demonstrated in which R_2' is sensitive to venous cerebral blood volume (CBV) and deoxyhaemoglobin concentration (He and Yablonskiy, 2007; He et al., 2008). Recently the approach of Davis et al. (1998) and Hoge et al. (1999a) has been extended to use both hypercapnia and hyperoxia induced CBF and BOLD signal changes to estimate venous deoxyhaemoglobin concentration and thus OEF and absolute $CMRO_2$ (Bulte et al., 2012; Gauthier and Hoge, 2012). It is this approach that we develop in the current work.

The methods presented here and those of Bulte et al. (2012) and Gauthier and Hoge (2012) rely on increasing venous blood oxygenation to increase the BOLD signal by raising (i) CBF and (ii) the arterial oxygen content. Crucially, the additional oxygen carried in arterial blood both bound to haemoglobin and in solution, under isometabolic conditions, manifests as an increase in venous blood oxygenation. Similarly, increasing CBF using an isometabolic hypercapnic challenge also increases venous blood oxygenation. The present study aims to demonstrate, using interleaved hypercapnic and hyperoxic respiratory challenges similar to those of Bulte et al. (2012), the measurement of absolute $CMRO_2$ at rest and during presentation of a continuous high contrast visual stimulus to provide an elevated absolute $CMRO_2$ to experimentally simulate long term alteration of cerebral metabolism. This absolute measurement is compared with a more conventional evaluation of stimulus-induced relative change in $CMRO_2$ (Davis et al., 1998).

Our computer-controlled system for administering respiratory challenges through dynamic end-tidal forcing (Wise et al., 2007) allows us to extend the interleaved approach to implement varying levels of hypercapnia simultaneously with intermittent hyperoxia. This combined respiratory challenge offers the potential to reduce the duration of the experiment. Simultaneous modulation of CBF and arterial oxygen levels would also introduce additional information with respect to an experiment in which hypercapnia and hyperoxia are induced separately. The CBF increase from hypercapnia is expected to also increase CBV to which a hyperoxia-induced BOLD signal change would be sensitive (Blockley et al., 2012a; Driver et al., 2012). We demonstrate that, using this combined approach and a model of BOLD signal incorporating the effects of increased CBF and arterial oxygen levels, we can uncover information about, the parameters in the commonly applied BOLD signal model, known as α, the exponent relating relative increases in CBF to CBV, and β, the exponent relating deoxyhaemoglobin concentration to the relaxation rate R_2^*, both of these model parameters being dependent on the cerebrovasculature.

Theory: calibration model

Our aim is to develop the form of the BOLD signal model as described by Davis et al. (1998) to yield the resting venous deoxyhaemoglobin concentration, $[dHb]_0$, thus offering a framework for the experimental measurement of absolute $CMRO_2$. Appendix A describes the fuller considerations behind the model summarised here. Our model description is a more general version of that expressed by Bulte et al. (2012), allowing for simultaneous modulation of CBF and arterial oxygen content (CaO_2) and is similar to that of Gauthier and Hoge (2012). The model reduces to the hypercapnia (Davis et al., 1998; Hoge et al., 1999a) and hyperoxia (Chiarelli et al., 2007) based models for calibration of BOLD signal when arterial oxygen levels and CBF are held constant respectively. In addition to being applied to isolated periods of hypercapnia (elevated CBF) or hyperoxia (elevated CaO_2), we derive signal relationships for the simultaneous variation of CBF (through hypercapnia) and arterial oxygen content (through hyperoxia), thus exploring the additional information which may be extracted from simultaneously acquired BOLD and CBF signal.

In the model of Davis and Hoge (Davis et al., 1998; Hoge et al., 1999a), considering principally extravascular BOLD contrast, relative BOLD signal change ($\Delta S/S_0$) is described by:

$$\frac{\Delta S}{S_0} = M\left\{1-\left(\frac{CBV}{CBV_0}\right)\left(\frac{[dHb]}{[dHb]_0}\right)^{\beta}\right\} \tag{1}$$

where M can be considered as the BOLD signal change elicited by the total elimination of deoxyhaemoglobin from the image voxel and CBV_0 is the baseline BOLD-relevant blood volume, normally considered to be principally venous:

$$M = TE \cdot A \cdot CBV_0 \cdot [dHb]_0^{\beta} \tag{2}$$

β is a constant that depends on vessel size and geometry as well as magnetic field strength, TE is the echo time and A is a field-dependent constant. A further power law relationship is assumed between relative changes in blood volume and cerebral blood flow, governed by, α, the Grubb coefficient (Grubb et al., 1974):

$$\left(\frac{CBV}{CBV_0}\right) = \left(\frac{CBF}{CBF_0}\right)^{\alpha}. \tag{3}$$

We assume that with physiologically moderate modulation of CBF by hypercapnia and the total arterial oxygen content (CaO_2) by hyperoxia, brain tissue oxygen consumption remains unaltered (Chen and Pike, 2010a). With hyperoxia additional oxygen is largely dissolved in arterial blood plasma and therefore manifests as increased venous oxygen saturation (SvO_2). The conservation of oxygen allows us to derive (see Appendix A) an expression for the venous deoxyhaemoglobin concentration with respect to baseline conditions (subscript 0):

$$\frac{[dHb]}{[dHb]_0} = \frac{CBF_0}{CBF} - \frac{1}{[dHb]_0}\left\{\frac{1}{\phi}\left(CaO_2 - \left(\frac{CBF_0}{CBF}\right)CaO_2|_0\right) + [Hb]\left(\frac{CBF_0}{CBF}-1\right)\right\} \tag{4}$$

where ϕ is the O_2 carrying capacity of haemoglobin (1.34 ml O_2/g_{Hb}) and we assume the concentration of haemoglobin to be [Hb] = 15 g Hb $dl^{-1}{}_{blood}$.

Eqs. (1), (3) and (4) together permit M and $[dHb]_0$ to be estimated based on iso-metabolic modulation of CBF and CaO_2. CBF can be measured simultaneously with BOLD signal using arterial spin labelling and CaO_2 is estimated from arterial partial pressure of oxygen (PaO_2, Appendix A), which in subjects with normal pulmonary function can reasonably be represented with only a small systematic error by the partial pressure of end-tidal O_2 ($P_{ET_{O_2}}$) (Bulte et al., 2007b). $[dHb]_0$ leads to oxygen extraction fraction (OEF), assuming normal values for [Hb] or measuring them and therefore allowing cerebral metabolic oxygen consumption to be calculated:

$$CMRO_2 = CaO_2 \cdot OEF \cdot CBF. \tag{5}$$

The use of a flexible system for manipulating and controlling independently arterial concentrations of CO_2 and O_2 permits the experimental exploitation of the combined relationships Eqs. (1), (3) and (4). We have previously implemented such an end-tidal forcing system for respiratory gas control in the MR environment and this is used in the present investigation (Wise et al., 2007). The joint manipulation of oxygen and carbon dioxide levels as well as permitting the estimation of $[dHb]_0$ and M has the potential to yield information on the exponents α and β through Eqs. (1), (3) and (4).

We consider a specific case applied in the present investigation in which BOLD signal changes resulting from modulation of arterial oxygen content are simultaneously modulated by hypercapnia induced changes in CBF. Considering two different levels of CBF (CBF_1 and CBF_2) the ratio of the superimposed arterial oxygen induced changes in BOLD signal can be approximated by:

$$\frac{\Delta S_{1,O_2}}{\Delta S_{2,O_2}} = \left(\frac{CBF_1}{CBF_2}\right)^{1+\alpha-\beta} \tag{6}$$

where $\Delta S_{i,O_2} = \frac{\Delta S_i}{\Delta CaO_2|_i}$ is the hyperoxia-induced BOLD signal change normalized to the change in total arterial oxygen content caused by hyperoxia, measured at the ith CBF level. This relationship is derived in Appendix A and we use it to constrain estimates of α and β through experimental estimation of the exponent $\eta = (1+\alpha-\beta)$.

Methods

Respiratory and stimulation protocols

Eleven subjects (5 female, age: 29 ± 5.3 years) were scanned having given informed written consent. Experimental procedures were approved by the local institutional ethical review committee.

Volunteers underwent 4 scans the order of A–C being randomised but with D always occurring last within the scan session:

A. Interleaved hypercapnia and hyperoxia at rest (19 min) (Fig. 1)
B. Interleaved hypercapnia and hyperoxia with continuous visual stimulation (19 min) (Fig. 1)
C. Visual stimulation (90 s ON, 90 s OFF, duration 10 min 30 s equivalent to 3 ½ cycles, starting and finishing with OFF)
D. Combined hypercapnia and hyperoxia at rest (13 min) (Fig. 2)

Visual stimulation consisted of a full contrast reversing checkerboard pattern (8 Hz) and, apart from its duration, was identical for scans B and C. The rest condition consisted of eyes open fixation on a central cross on the in-scanner display screen.

Respiratory challenges were administered using a system of end-tidal forcing (Wise et al., 2007) which offers independent control of partial pressures of end-tidal oxygen and carbon dioxide ($P_{ET_{O_2}}$ and $P_{ET_{CO_2}}$ respectively). The end-tidal forcing system comprised a laptop personal computer using BreatheDmx software (Department of Physiology, Anatomy and Genetics, Oxford University, UK) to monitor end-tidal expired gas levels and calculate the inspired partial pressures required to achieve the desired target. The gas mixtures were delivered at a total flow rate of 30 litres per minute (lpm) through a fast gas mixing chamber connected to a tight-fitting face-mask worn by the volunteer (Quadralite, Intersurgical, Wokingham, Berkshire, UK). The respiratory circuit included a reservoir on the expired limb to permit re-breathing in the event that the instantaneous inspiratory rate exceeded 30 lpm. Supplies of 10% CO_2 (balance air), 10% O_2 (balance N_2), 100% O_2 and air were delivered from cylinders to the gas mixing chamber which was placed as close as possible to the volunteer (on his/her chest) to minimise delays in delivery. Gas delivery was controlled by four mass flow controllers (MKS Instruments, Wilmington, MA, USA). Tidal gases, sampled from the volunteer's facemask and $P_{ET_{CO_2}}$ and $P_{ET_{O_2}}$, were measured using rapidly responding gas analysers (AEI Technologies, Pittsburgh, PA, USA). A complete description of the end-tidal forcing system can be found in Wise et al. (2007).

Before the commencement of scanning, the volunteer rested in the scanner for a minimum of 5 min whilst $P_{ET_{CO_2}}$ and $P_{ET_{O_2}}$ were monitored. Resting $P_{ET_{O_2}}$ and $P_{ET_{CO_2}}$ were used as the targets for the normoxic and normocapnic periods. The target profiles for $P_{ET_{CO_2}}$ and $P_{ET_{O_2}}$ for scans A and B are shown in Fig. 1a, whilst the target profiles for scan D are shown in Fig. 2a. During scan C the volunteer breathed medical air only without control of end-tidal CO_2 and O_2.

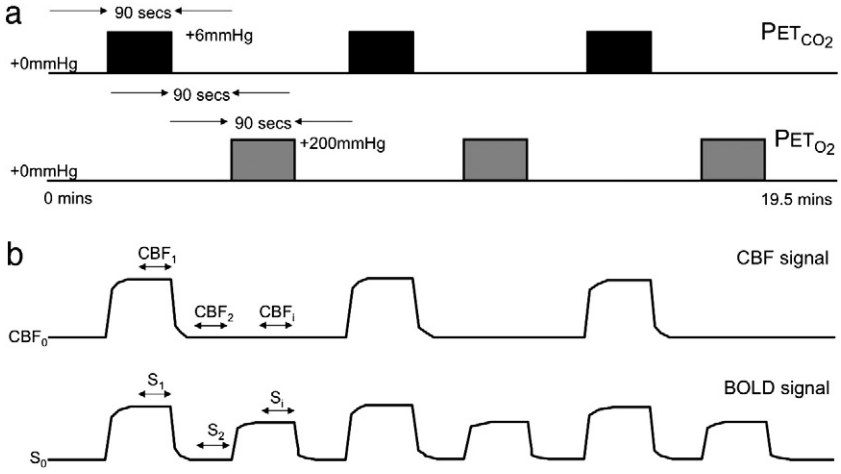

Fig. 1. Experimental design for scans A and B: interleaved hypercapnia and hyperoxia. a) Indicates the timing of hypercapnic and hyperoxic blocks (90 s duration) alternating with blocks of normocapnia and normoxia. For the normocapnic periods end-tidal CO_2 was held at 1 mm Hg above the resting value measured before the start of the scan to allow the dynamic end-tidal forcing system to perform its control (Wise et al., 2007). For hypercapnia and hyperoxia the targeted increases in end-tidal CO_2 and O_2 respectively are indicated. b) Shows, schematically, the increase of the CBF signal during hypercapnia and the increase of the BOLD signal during both hypercapnia and hyperoxia. For signal modelling mean CBF and BOLD signals for the final 44 s of each block were estimated, CBF_i and S_i respectively. The same experimental design was performed for scan A (rest) and scan B (continuous reversing visual checkerboard).

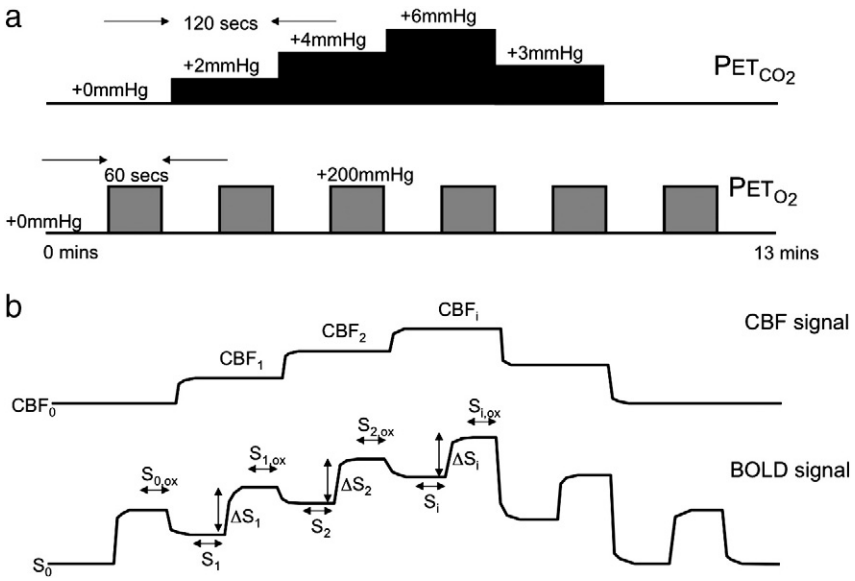

Fig. 2. Experimental design for scan D: combined hypercapnia and hyperoxia. a) Indicates the timing of the hypercapnic levels administered and the hyperoxic blocks. For the normocapnic periods end-tidal CO_2 was held at 1 mm Hg above the resting value measured before the start of the scan to allow the dynamic end-tidal forcing system to perform its control (Wise et al., 2007). For hypercapnia and hyperoxia the targeted increases in end-tidal CO_2 and O_2 respectively are indicated. b) Shows, schematically, the increase of the CBF and of the BOLD signals during both hypercapnia and hyperoxia. For signal modelling mean CBF and BOLD signals for the final 33 s of each oxygen level block were estimated, CBF_i and S_i respectively.

Respiration was monitored with a pneumatic belt around the chest. Pulse timing was collected from a pulse oximeter worn on the left hand. Physiological data were recorded with a computer-based data acquisition system (CED 1401, Cambridge, UK) for subsequent physiological noise correction of fMRI data.

MRI scanning

Image data were acquired on a 3 T whole body MRI system (GE Excite HDx, Milwaukee, WI) using an eight-channel receive-only head coil. Functional data were acquired using a pulsed arterial spin labelling (ASL) proximal inversion and control for off-resonance effects (PICORE), quantitative imaging of perfusion using a single subtraction (PICORE QUIPSS II) (Wong et al., 1998) imaging sequence (non-commercial). This sequence used a dual-echo gradient echo (GRE) readout (Liu et al., 2002) and spiral k-space acquisition (Glover, 1999) ($TE_1 = 3$ ms $TE_2 = 29$ ms, TR = 2.2 s, flip angle 90°, FOV 22 cm, matrix 64 × 64, 10 slices of 7 mm thickness with an inter-slice gap of 1 mm, $TI_1 = 700$ ms, $TI_2 = 1600$ ms for the most proximal slice, 10 cm inversion slab thickness, adiabatic hyperbolic secant inversion pulse, 10 mm gap between labelling slab and bottom slice, 10 cm QUIPSS II saturation band thickness). 532, 532, 286 and 354 repetitions (image volumes) were collected for scans A, B, C and D respectively. A separate single shot (M_0) scan was acquired with the same parameters as the functional runs to measure the equilibrium brain tissue magnetisation for purposes of calculating CBF. A whole brain T_1-weighted structural scan (fast spoiled gradient recalled echo, 1 × 1 × 1 mm voxels, TI/TR/TE = 450/7.8/3 ms) was acquired to facilitate registration of the functional data to the common standard space of the Montreal Neurological Institute (MNI).

Data analysis

Functional data pre-processing

The image data acquired from the first echo were used to calculate CBF, whilst those data from the second echo were used to examine changes in BOLD (T_2^* weighted) signal.

Physiological noise correction, (a modified RETROICOR), was applied with the first and second harmonics of both the cardiac and respiratory cycles being regressed from the data along with the interaction term of the first cardiac and respiratory harmonics (Glover et al., 2000; Harvey et al., 2008). The data were then pre-processed with motion correction (MCFLIRT (Jenkinson et al., 2002)), followed by high-pass filtering (cut off 8 s) using FSL tools (www.fmrib.ox.ac.uk/fsl). Interpolated surround subtraction of the ASL tag and control image time-series was performed to yield perfusion weighted time-series (Liu and Wong, 2005). To quantify CBF, the signal from CSF was measured from the fully relaxed scan to estimate the M_0 of blood. In-house software was used to convert the measured perfusion weighted signal to an estimate of CBF in ml/100 g/min by applying a standard single compartment model (Wong et al., 1998). The CBF estimates were adjusted for the likely reduction of the T_1 of arterial blood with increasing plasma concentration of paramagnetic O_2, according to the blood T_1 values quoted by Bulte et al. (2007b).

BOLD data were pre-processed with motion correction and high-pass filtering (cut off 540 s for scans A and B and 270 s for scan C with no high-pass filtering for scan D). Physiological noise correction was applied in the same manner as for the CBF data. Interpolated surround averaging of the tag and control images was performed to yield BOLD weighted time-series.

Both the CBF weighted and BOLD contrast data for the visual block-design scan C were analysed to identify significant visual stimulus-induced changes in CBF and BOLD signals using a linear modelling approach (FEAT within FSL) following the pre-processing described above. The data were brain extracted (Smith, 2002) and spatially smoothed with a Gaussian kernel of 5 mm. A box-car regressor with on/off periods of 90 s each, convolved with a single gamma function haemodynamic response function, was fitted to the data for each subject using fMRIB's Improved Linear Model (FILM) within FEAT (Woolrich et al., 2001). Parameter estimates were converted to Z statistics and thresholded at $Z > 2.3$ for both the CBF and the BOLD contrast data. The conjunction of supra-threshold voxels was used to define for each volunteer a functional region of interest in which both CBF and BOLD signals were significantly increased by the

visual stimulus for later use in establishing changes in $CMRO_2$ within this region.

Registration

Single-subject low-resolution functional images were co-registered to their corresponding high-resolution T_1 weighted structural images using fMRIB's linear image registration tool (FLIRT) with 6 degrees of freedom (Jenkinson and Smith, 2001). The T_1 weighted structural images were affine co-registered to the standard brain (Montreal Neurological Institute (MNI) — 152 template) using FLIRT (12 degrees of freedom) followed by refinement by nonlinear registration using fMRIB's nonlinear image registration tool (FNIRT) (www.fmrib.ox.ac.uk/fsl).

Metabolic calculations and model fitting

Following registration to the common standard space of the MNI, region of interest time-series of CBF and BOLD weighted data (scans A, B, C and D) were extracted for each individual for global grey matter, thalamus, anterior cingulate cortex, insular cortex, frontal cortex, parietal cortex and occipital cortex. Regions were defined from the 50% threshold of the probabilistic map of the tissue priors available in the fMRIB software library (www.fmrib.ox.ac.uk/fsl, Harvard–Oxford cortical and subcortical atlases). Further time-series were also extracted from scans A, B and C for the functional visual region of interest defined from scan C as described above.

For scans A and B (interleaved hypercapnia and hyperoxia), for each region of interest's time-series, time averaged relative CBF (CBF/CBF_0) and BOLD signal ($\Delta S/S_0$) were calculated for each final 44 s period of each 90 s respiratory block, namely, normocapnia and normoxia, hypercapnia and normoxia, and normocapnia and hyperoxia (Fig. 1b). For scan D (combined hypercapnia and hyperoxia) relative CBF and BOLD signals were calculated for the final 33 s period of each respiratory block (Fig. 2b). The mean arterial oxygen content CaO_2 was calculated from the $P_{ET_{O_2}}$ data for the same time periods (Eq. (A11)).

Interleaved design — absolute $CMRO_2$

The model described by Eqs. (A1) and (A10) was fitted to the whole-brain grey matter and regional data using a Bayesian framework (described below) to yield M and SvO_2 for scan A (rest), permitting calculation of absolute $CMRO_2$ (Fig. 3, blue analysis pathway). This was repeated for previously used combinations of α and β, (α, β) = (0.38, 1.5) and (0.14, 0.91) (Griffeth and Buxton, 2011); and for whole grey matter only (0.2, 1.3) (Bulte et al., 2012) and (0.18, 1.5) (Gauthier and Hoge, 2012). Given that scan D is able to yield information relating the hyperoxia-related BOLD signal changes to different levels of hypercapnia-modulated CBF, fitting data from scan D to Eq. (A18) we estimated i) α, holding β constant at 1.5 or 0.91, and ii) α and β, allowing them both to vary. We used these additional combinations of α and β to estimate M and SvO_2 from scan A (Fig. 3, orange analysis pathway). Using fixed combinations of α and β, (α, β) = (0.38, 1.5) and (0.14, 0.91) we also estimated M and SvO_2 and therefore absolute $CMRO_2$ in the functionally defined visual region of interest from scans A (rest) and B (visual stimulation) (Fig. 3, blue and purple analysis pathways).

Visual task — relative changes in $CMRO_2$

Having estimated M from the hypercapnia component of scan A (rest), within the visual region of interest using Eq. (A1) only, assuming an isometabolic vascular stimulus from the hypercapnia, we calculated the fractional increase in $CMRO_2$ during scan C using Eq. (1), according to the conventional hypercapnic calibration approach described by Hoge et al. (1999a) and Davis et al. (1998) (Fig. 3, green analysis pathway). This allowed us to compare the oxygen consumption increase for a short stimulus with that for the long duration stimulus of scan B.

Combined design — absolute $CMRO_2$

The model described by Eqs. (A1) and (A10) was fitted to the whole grey matter and regional data to yield M and SvO_2 for scan D (rest with combined hypercapnia and hyperoxia), permitting calculation of absolute $CMRO_2$. This was repeated for

i) previously used combinations of α and β, (α, β) = (0.38, 1.5) and (0.14, 0.91); and for whole grey matter only (0.2, 1.3) (Bulte et al., 2012) and (0.18, 1.5) (Gauthier and Hoge, 2012).
ii) fixed β = 1.5 whilst fitting for α
iii) fixed β = 0.91 whilst fitting for α and
iv) fitting for both α and β.

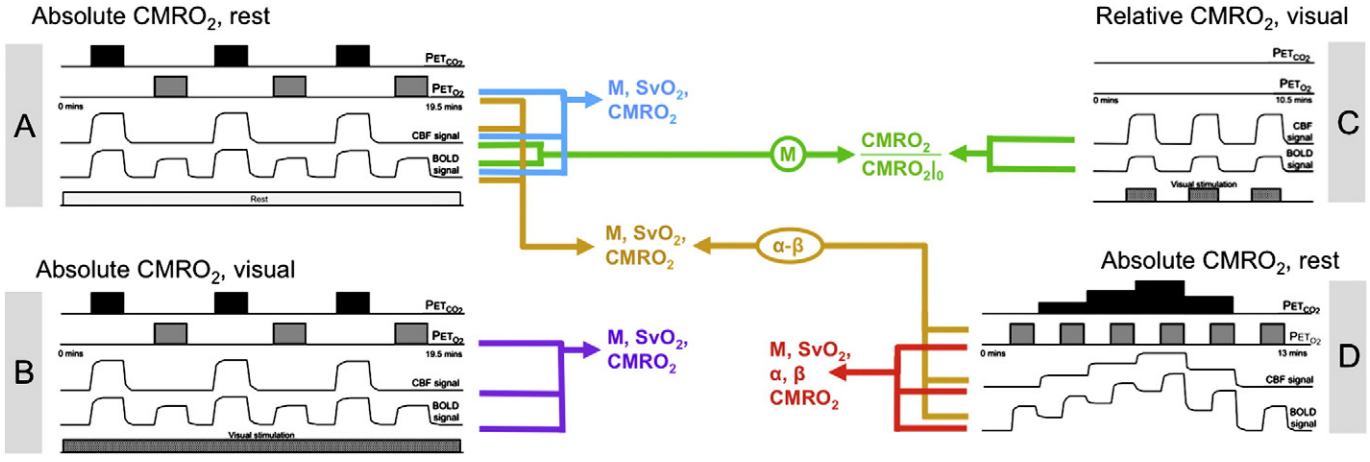

Fig. 3. Summary of experiments and analysis routes to establish cerebro-metabolic parameters. Scans A and B followed the same experimental design of interleaved hypercapnic and hyperoxic stimuli (Fig. 1) with A being performed at rest and B having the continuous high-contrast visual stimulus. The blue and purple analysis routes are the same for scans A and B using assumed values of α and β from the literature. Scan C used no respiratory challenges and presented only 90 s blocks of visual stimulation interleaved with blocks of rest, in order to measure the visually induced increase in $CMRO_2$ relative to rest (baseline), following the green analysis route having established M from the hypercapnic calibration in scan A and using assumed values of α and β. Scan D was performed at rest with combined hypercapnic and hyperoxic respiratory challenges (Fig. 2). By virtue of the measurement of hyperoxia induced BOLD contrast at different levels of CBF, we estimated M, SvO_2, $CMRO_2$, α and β from scan D (red analysis route). Using the information from modulation of BOLD signal in scan D we also estimated α − β to constrain values of α and β for applying to data from scan A (orange analysis route).

Parameter estimation from this model of M, SvO_2, α and β was also performed voxel-wise within grey matter for the combined resting hypercapnia and hyperoxia scan (D) yielding maps of OEF, $CMRO_2$, CBF, α and β (Fig. 3, red analysis pathway).

Model fitting using a Bayesian framework

A Bayesian framework was used to fit the model to the data. Priors for M, SvO_2, α and β were generated as normal probability density functions centred around initial estimates of 0.08, 0.5, 0.3 and 1.4 with broad standard deviations of 0.02, 0.1, 0.1 and 0.2 respectively. When in a particular analysis, a certain variable was fixed (e.g., $\beta = 1.5$), a delta function of the fixed value was used. By applying Bayes' rule to the first time points of averaged data (relative BOLD change, relative CBF change and CaO_2), posterior probability distributions of the four variables, M, SvO_2, α and β, were generated after integrating over the ranges 0.01–0.15, 0.2–0.8, 0.1–0.5 and 0.8–2.0 respectively (chosen to be beyond the extremes of physiologically plausible values). These posterior distributions were used as the priors for calculations with the second time point of averaged data and so on until a final posterior distribution for each of the 4 variables was obtained. The maxima of these probability distribution functions provided the estimates of M, SvO_2, α and β for that subject/voxel. $CMRO_2$ was calculated using Eq. (5). For some subjects/voxels, one or more of the variables (M, SvO_2, α and β) were estimated to be at the boundary of an integration range. If this was the case, the subject/voxel was excluded from the tables and figures.

Results

Table 1 indicates for whole brain grey matter the CBF and fitted values, from the interleaved hypercapnia and hyperoxia design, of M and SvO_2, along with the calculated absolute $CMRO_2$. Results for different combinations of (α, β) are presented using literature values in the blue analysis pathway (Fig. 3), (0.38, 1.50), (0.2, 1.3), (0.18, 1.5) and (0.14, 0.91) and also from the orange analysis pathway (Fig. 3) (α_D, 1.5), (α_D, 0.91) and ($\alpha_{D'}$, $\beta_{D'}$), where $\alpha_{D'}$ and $\beta_{D'}$ indicate values estimated by fitting the exponent, η, in Eq. (6). When β is fixed, α_D is simply equal to $\eta - (1 - \beta)$. When β is allowed to vary, α_D and β_D are fit within the Bayesian framework with the constraint that $\eta = (1+\alpha_D - \beta_D)$.

Table 1 also shows for whole brain grey matter the CBF and fitted values, from the combined hypercapnia and hyperoxia design (scan D), of M and SvO_2, along with the calculated absolute $CMRO_2$. Results are presented (red analysis pathway, Fig. 3) for literature based combinations of (α, β), (0.38, 1.50), (0.2, 1.3), (0.18, 1.5) and (0.14, 0.91) and also (α, 1.5), (α, 0.91) and (α, β), where α and β indicate values estimated along with M and SvO_2 using the full signal model (Eqs. (1), (3) and (4)).

Estimates of regional brain SvO_2, along with $CMRO_2$ are given in Table 2 for the interleaved (resting scan A) and combined designs (resting scan D) (blue and red analysis pathways respectively from Fig. 3). For the combined calibration, α and β were estimated (red analysis route, Fig. 3) to be approximately 0.3 and 1.3 respectively. For the interleaved design SvO_2 (OEF) lies in the range 0.5 (0.5)–0.63 (0.37), whilst for the combined design SvO_2 (OEF) lies in the range 0.58 (0.42)–0.64 (0.36), with correspondingly lower estimates of $CMRO_2$ for the combined design than for the interleaved design.

From the combined carbon dioxide and oxygen modulation (scan D, red analysis route, Fig. 3) we estimated voxel-wise, SvO_2 (and thus OEF), M, $CMRO_2$, CBF, α and β and these parameters are shown as group average maps in standard (MNI) space over grey matter in Figs. 4a–g. In some voxels estimation of parameters failed by reaching the boundary conditions and these locations were excluded from the group mean. The resulting group average maps of the fitted parameters therefore have a different number of subjects, shown in Fig. 4h, contributing to the plotted mean value at each voxel.

Focussing on the region of interest defined by the visual task in scan C (lying in visual cortex), Table 3 shows the fitted M and SvO_2 estimates for the resting scan (A) and continuous visual stimulus (scan B), for $(\alpha, \beta) = (0.38, 1.50)$ and (0.14, 0.91) (blue and purple analysis routes respectively, Fig. 3). CBF, SvO_2 and $CMRO_2$ were seen to increase, for both combinations of α and β, during the continuous visual stimulation. Paired *t*-tests showed that the CBF increase in visual cortex was significant ($p \leq 0.01$). The SvO_2 and $CMRO_2$ increases in visual cortex were significant ($p \leq 0.05$) for $(\alpha, \beta) = (0.14, 0.91)$ and for $(\alpha, \beta) = (0.38, 1.50)$ (across the 6 common successfully fitted subjects). For these 6 subjects, the ratios of absolute $CMRO_2$ between visual activation and rest were 1.13 ± 0.09 ($\alpha = 0.38$, $\beta = 1.5$) and 1.11 ± 0.08 ($\alpha = 0.14$, $\beta = 0.91$). A control region was also examined from scans A and B, the anterior cingulate cortex, as this was not expected to show an appreciable response to the low-level visual stimulus. CBF, SvO_2 and absolute $CMRO_2$ did not appear to show a stimulus related increase in this region (changes were statistically insignificant across the 9 common successfully fitted subjects). Relative changes in $CMRO_2$ were examined from the 90 s block stimuli presented in scan

Table 1
Whole-brain grey matter estimated vascular and metabolic parameters at rest. CBF estimates derive from the normoxic, normocapnic baseline period. *Interleaved* refers to scan A and indicates that hypercapnia and hyperoxia were administered at different times. *Combined* refers to scan D and indicates that graded hypercapnia and hyperoxia were administered simultaneously. Underlined α and β values indicate that they are fixed to values reported in previous works and not fitted from the current experimental data. Where β was fixed for the interleaved design, α was given by the estimation of $(\alpha - \beta)$ from Eq. (6) using the data from scan D (combined hypercapnia and hyperoxia). The number (#) of subjects indicates in how many subjects the parameter estimation procedure was successful and therefore the number contributing to the reported mean. The analysis route refers, by colour code, to the schematic of the analysis pipelines indicated in Fig. 3. Values are quoted as mean ± standard deviation.

Scan	CBF (ml/100 g/min)	M	SvO_2	$CMRO_2$ (μmol/100 g/min)	Alpha	Beta	#subs	Analysis route
Interleaved	55.5 ± 10.9	0.067 ± 0.024	0.50 ± 0.12	222 ± 82	0.38	1.50	10/11	Blue
	55.5 ± 10.9	0.069 ± 0.025	0.53 ± 0.12	210 ± 80	0.20	1.30	10/11	Blue
	54.9 ± 11.3	0.064 ± 0.023	0.50 ± 0.10	222 ± 81	0.18	1.50	9/11	Blue
	55.5 ± 10.9	0.089 ± 0.029	0.54 ± 0.10	206 ± 71	0.14	0.91	10/11	Blue
	55.5 ± 10.9	0.075 ± 0.025	0.55 ± 0.10	204 ± 70	0.50 ± 0.22	1.50	10/11	Orange
	55.3 ± 12.0	0.087 ± 0.024	0.63 ± 0.10	167 ± 66	−0.08 ± 0.23	0.91	8/11	Orange
	55.5 ± 10.9	0.077 ± 0.028	0.58 ± 0.09	188 ± 65	0.32 ± 0.02	1.31 ± 0.23	10/11	Orange
Combined	55.9 ± 11.6	0.078 ± 0.021	0.58 ± 0.14	185 ± 53	0.38	1.50	11/11	Red
	55.7 ± 12.2	0.084 ± 0.020	0.59 ± 0.13	178 ± 48	0.20	1.30	10/11	Red
	55.7 ± 12.2	0.073 ± 0.017	0.60 ± 0.13	177 ± 48	0.18	1.50	10/11	Red
	55.9 ± 11.6	0.101 ± 0.025	0.64 ± 0.13	156 ± 43	0.14	0.91	11/11	Red
	55.9 ± 11.6	0.076 ± 0.018	0.58 ± 0.13	183 ± 50	0.34 ± 0.06	1.50	11/11	Red
	55.2 ± 12.0	0.107 ± 0.013	0.62 ± 0.11	164 ± 36	0.27 ± 0.08	0.91	10/11	Red
	55.9 ± 11.6	0.084 ± 0.012	0.58 ± 0.12	184 ± 45	0.33 ± 0.06	1.35 ± 0.13	11/11	Red

Table 2
Regional grey matter estimated vascular and metabolic parameters at rest. CBF estimates derive from the normoxic, normocapnic baseline period. *Interleaved* refers to scan A and indicates that hypercapnia and hyperoxia were administered at different times. *Combined* refers to scan D and indicates that graded hypercapnia and hyperoxia were administered simultaneously. Underlined α and β values indicate that they are fixed to values reported in previous works and not fitted from the current experimental data. The number (#) of subjects indicates in how many subjects the parameter estimation procedure was successful and therefore the number contributing to the reported mean. The analysis route refers, by colour code, to the schematic of the analysis pipelines indicated in Fig. 3. Values are quoted as mean ± standard deviation.

Scan	CBF (ml/100 g/min)	M	SvO_2	$CMRO_2$ (μmol/100 g/min)	Alpha	Beta	#subs	Analysis route
Interleaved								
Occipital	68.2 ± 16.0	0.056 ± 0.028	0.52 ± 0.11	263 ± 105	0.38	1.50	9/11	Blue
Thalamus	63.9 ± 17.3	0.058 ± 0.018	0.58 ± 0.12	219 ± 103			7/11	Blue
Acc	58.7 ± 11.5	0.061 ± 0.020	0.52 ± 0.09	225 ± 66			10/11	Blue
Frontal	47.3 ± 10.1	0.054 ± 0.024	0.50 ± 0.11	189 ± 56			10/11	Blue
Insula	64.5 ± 10.7	0.056 ± 0.019	0.56 ± 0.14	233 ± 97			9/11	Blue
Parietal	46.1 ± 10.2	0.061 ± 0.026	0.52 ± 0.08	179 ± 59			10/11	Blue
Grey matter	55.5 ± 10.9	0.067 ± 0.024	0.50 ± 0.12	222 ± 82			10/11	Blue
Occiptal	65.9 ± 16.6	0.070 ± 0.033	0.57 ± 0.12	229 ± 100	0.14	0.91	10/11	Blue
Thalamus	63.9 ± 17.3	0.079 ± 0.022	0.60 ± 0.12	211 ± 93			7/11	Blue
Acc	58.7 ± 11.5	0.081 ± 0.024	0.54 ± 0.09	215 ± 64			10/11	Blue
Frontal	47.3 ± 10.1	0.073 ± 0.031	0.52 ± 0.08	181 ± 45			10/11	Blue
Insula	63.6 ± 11.1	0.080 ± 0.020	0.56 ± 0.12	231 ± 92			8/11	Blue
Parietal	46.1 ± 10.2	0.081 ± 0.031	0.56 ± 0.06	165 ± 51			10/11	Blue
Grey matter	55.5 ± 10.9	0.089 ± 0.029	0.54 ± 0.10	206 ± 71			10/11	Blue
Combined								
Occipital	65.3 ± 17.0	0.078 ± 0.014	0.55 ± 0.11	239 ± 77	0.32 ± 0.05	1.34 ± 0.12	11/11	Red
Thalamus	60.7 ± 13.6	0.082 ± 0.011	0.61 ± 0.11	193 ± 60	0.35 ± 0.05	1.28 ± 0.16	11/11	Red
Acc	54.5 ± 15.3	0.077 ± 0.019	0.57 ± 0.12	185 ± 61	0.32 ± 0.05	1.37 ± 0.13	11/11	Red
Frontal	46.9 ± 14.4	0.071 ± 0.014	0.60 ± 0.11	145 ± 48	0.35 ± 0.04	1.28 ± 0.08	11/11	Red
Insula	67.4 ± 16.1	0.078 ± 0.017	0.57 ± 0.08	231 ± 49	0.34 ± 0.06	1.31 ± 0.16	9/11	Red
Parietal	43.4 ± 11.3	0.083 ± 0.011	0.61 ± 0.11	137 ± 45	0.35 ± 0.07	1.29 ± 0.19	9/11	Red
Grey matter	55.9 ± 11.6	0.084 ± 0.012	0.58 ± 0.12	184 ± 45	0.33 ± 0.06	1.35 ± 0.13	11/11	Red

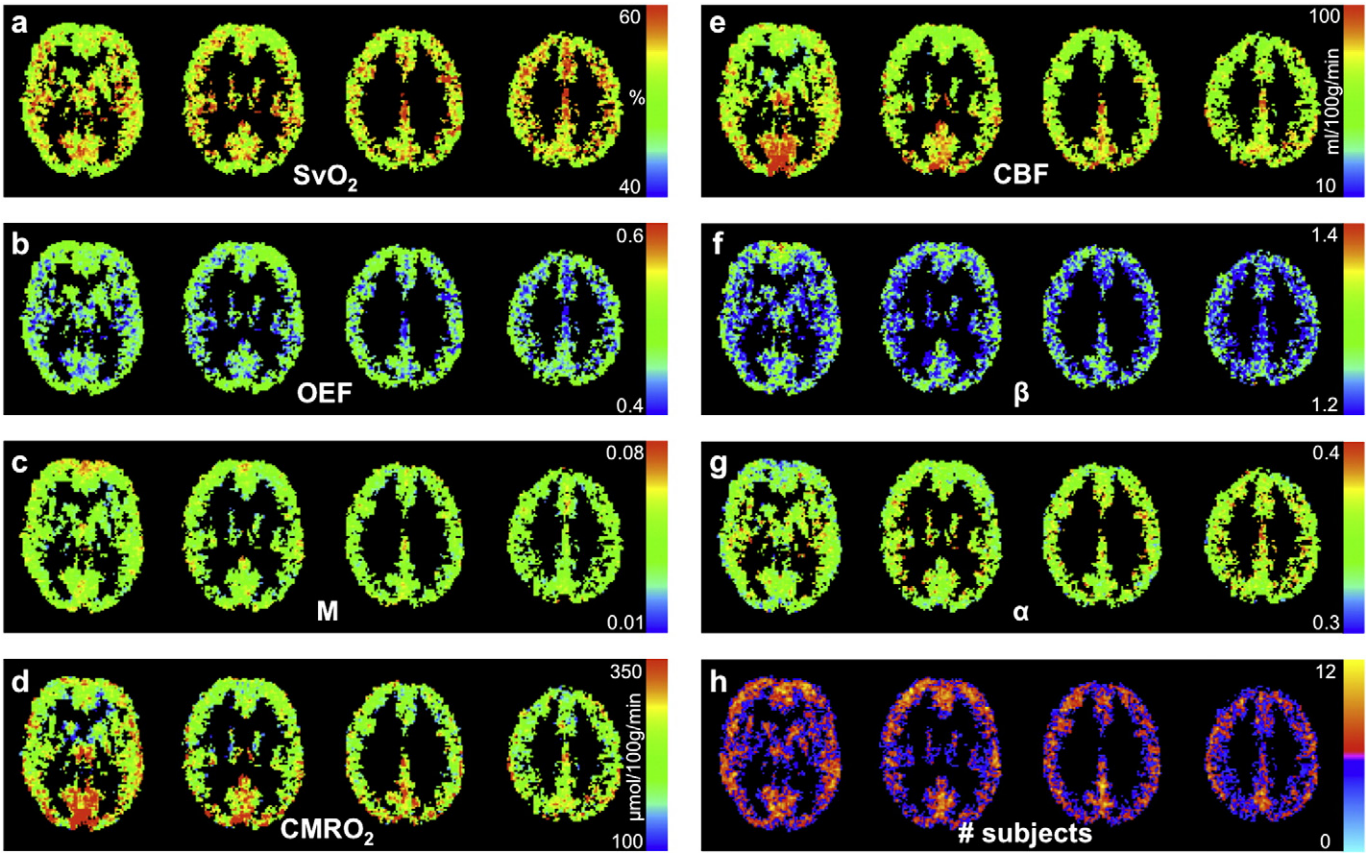

Fig. 4. Group mean maps of estimated cerebrovascular and cerebrometabolic parameters. a) Venous oxygen saturation (SvO_2), b) oxygen extraction fraction (OEF), c) M, the parameter describing the local maximum fractional BOLD signal increase in the absence of venous deoxyhaemoglobin, d) cerebral metabolic rate of oxygen consumption ($CMRO_2$) e) cerebral blood flow (CBF), f) β, the exponent relating R_2* relaxation rate constant to the concentration of deoxyhaemoglobin g) α, the exponent relating fractional increases in (venous) cerebral blood volume, relevant for generating BOLD signal contrast, to fractional increases in cerebral blood flow and h) a map of the number of subjects from the cohort of 11 who contribute data to the mean value at each voxel. Note that in some voxels not all subjects contribute as the parameter estimation was unreliable in those voxels in those subjects. Values are reported in grey matter only in which the CBF estimates were thought to be more reliable than in white matter. Data is from scan D, the combined hypercapnia, hyperoxia protocol.

Table 3
Regional estimated vascular and metabolic parameters at rest and during continuous visual stimulation with a high contrast visual checkerboard. CBF estimates derive from the normoxic, normocapnic baseline period. *Rest* refers to scan A and *Task* refers to scan B in which there was a high-contrast continuously reversing checkerboard. The *Visual* region of interest was defined functionally from scan C. A control region, anterior cingulate cortex (*ACC*) is also presented. Underlined α and β values indicate that they are fixed to values reported in previous works and not fitted from the current experimental data. The number (#) of subjects indicates in how many subjects the parameter estimation procedure was successful and therefore the number contributing to the reported mean. The analysis route refers, by colour code, to the schematic of the analysis pipelines indicated in Fig. 3. Values are quoted as mean ± standard deviation.

	CBF (ml/100 g/min)	M	SvO_2	$CMRO_2$ (μmol/100 g/min)	Alpha	Beta	#subs	Analysis route
Visual cortex								
Rest	80.8 ± 18.1	0.067 ± 0.033	0.52 ± 0.09	311 ± 103	0.38	1.50	8/11	Blue
Task	101.8 ± 27.4	0.069 ± 0.028	0.55 ± 0.14	375 ± 163			10/11	Purple
ACC								
Rest	58.7 ± 11.5	0.061 ± 0.020	0.52 ± 0.09	225 ± 66			10/11	Blue
Task	57.4 ± 11.5	0.056 ± 0.026	0.52 ± 0.13	227 ± 91			9/11	Purple
Visual cortex								
Rest	80.8 ± 18.1	0.086 ± 0.036	0.54 ± 0.06	294 ± 83	0.14	0.91	8/11	Blue
Task	99.9 ± 28.3	0.081 ± 0.015	0.61 ± 0.08	315 ± 117			9/11	Purple
ACC								
Rest	58.7 ± 11.5	0.081 ± 0.024	0.54 ± 0.09	215 ± 64			10/11	Blue
Task	57.4 ± 11.5	0.079 ± 0.033	0.54 ± 0.13	216 ± 94			9/11	Purple

C. The M parameter was estimated from the hypercapnia component of scan A for the visual region of interest, according to Eq. (1), and was used to estimate the relative increase in $CMRO_2$ with blocks of 90 s visual stimulation (scan C, green analysis route, Fig. 3) (Table 4). This increase was highly statistically significant ($p = 10^{-10}$).

To examine the possibility of slow changes in the cortical response to the long-duration visual stimulus we plotted the normocapnic, normoxic baseline period CBFs (relative to the first normocapnic, normoxic period) in the visual region of interest for scans A (rest) and B (stimulation) (Fig. 5). There was a significant difference in the slopes of a CBF regression with time in the stimulation scan versus the rest scan, indicating a significant reduction of CBF over the ~20 minute continuous stimulus in the visual cortex ($p < 0.05$, two-tailed paired *t*-test between CBF-time regression slopes for rest and stimulation scans, 11 subjects).

Discussion

We have demonstrated the measurement of absolute $CMRO_2$ using two different respiratory manipulation protocols and the simultaneous collection of T_2^* weighted and ASL perfusion weighted data, by exploiting the model of Davis et al. (1998) and Hoge et al. (1999a) extended to describe T_2^* weighted signal changes resulting from assumed isometabolic hyperoxia and hypercapnia. Our *combined* approach, namely the simultaneous modulation of arterial oxygen and carbon dioxide, yields additional information concerning MR bio-physical vascular properties (parameters α and β), compared to the previously demonstrated methods of Bulte et al. (2012) and Gauthier and Hoge (2012), that have assumed literature values of α and β. We have also demonstrated for the first time a change in absolute $CMRO_2$ associated with a continuous visual task, which can be thought of as an elevated absolute $CMRO_2$, offering the proof of concept that these quantitative fMRI methods have the potential to characterise long term changes in brain oxygen metabolism and thus opening the way to studies of brain diseases and treatment interventions.

The earlier methods for estimating stimulus-induced relative changes in $CMRO_2$ using hypercapnia (Davis et al., 1998; Hoge et al., 1999a), rely on establishing the BOLD signal change induced by an iso-metabolic and known increase in CBF. With the model proposed in those works, a calibration parameter M, was defined which is often interpreted at the maximum possible BOLD signal increase at very high (non-physiological) CBF in the limit at which all deoxyhaemoglobin is considered to be washed out of the vasculature ([dHb] = 0). The model (Eq. (1)) contains the term dependent on the ratio of (venous) deoxyhaemoglobin concentration during task [dHb] to that during rest $[dHb]_0$, a term which depends on the task-induced relative change in $CMRO_2$. Instead of applying this model to stimulus-induced changes in $CMRO_2$, it has been adapted here to measure absolute OEF and thus $CMRO_2$, by inducing a known change in the venous deoxyhaemoglobin concentration through the addition of oxygen to arterial blood (hyperoxia). The increase in oxygen carried in arterial blood is estimated from the partial pressure of oxygen in arterial blood. This second mechanism for modulating the BOLD signal based on a known change in oxygen, when combined with a hypercapnic CBF modulation, leaves the principal unknown as the venous deoxyhaemoglobin concentration at normocapnia and normoxia ($[dHb]_0$ in Eq. (1)), permitting OEF to be estimated.

Our global estimates of $CMRO_2$ (Table 1) tend to be somewhat larger than typical values in the literature quoted from PET. Typical values from ^{15}O PET in cerebral cortical regions are 136 ± 10 μmol/100 g/min albeit in an older cohort (52 ± 15 years) (Ito et al., 2004) and approximately 128–149 μmol/100 g/min depending on cortical region and in a cohort with a wide age range, from 22 to 82 years (Leenders et al., 1990). Extrapolating from data showing the variation of $CMRO_2$ with age in a middle cerebral artery supplied cortical region (Ibaraki et al., 2010) (Fig. 2), one might expect approximately 150 μmol/100 g/min in the present, fairly young, cohort. Comparisons with such PET studies are difficult because of the inter-regional differences and the probable greater effect of white matter partial volume reducing the estimates of grey matter $CMRO_2$ from PET. Our combined hyperoxia

Table 4
Regional (visual cortical) estimated visual stimulus-induced increases in CBF and $CMRO_2$ relative to rest. These estimates derive from scan C in which a 90 s reversing visual checkerboard stimulus was repeatedly presented. The region of interest was defined functionally from tissue showing a significant BOLD and CBF response to the visual stimulus. CBF/CBF_0 indicates CBF during the task relative to baseline and similarly for $CMRO_2$. M was calculated from scan A using the hypercapnic calibration. *n* is defined by the ratio of stimulus induced fractional changes in CBF to stimulus induced fractional changes in $CMRO_2$. All subjects contributed to these estimates. The analysis route refers, by colour code, to the schematic of the analysis pipelines indicated in Fig. 3. Values are quoted as mean ± standard deviation.

Relative $CMRO_2$	M	$\frac{CBF}{CBF_0}$	$\frac{CMRO_2}{CMRO_{2\|0}}$	*n*	Analysis route
$\alpha = 0.38, \beta = 1.5$	0.114 ± 0.063	1.391 ± 0.066	1.161 ± 0.056	2.73 ± 1.11	Green
$\alpha = 0.14, \beta = 0.91$	0.160 ± 0.090	1.391 ± 0.066	1.183 ± 0.065	2.46 ± 1.09	Green

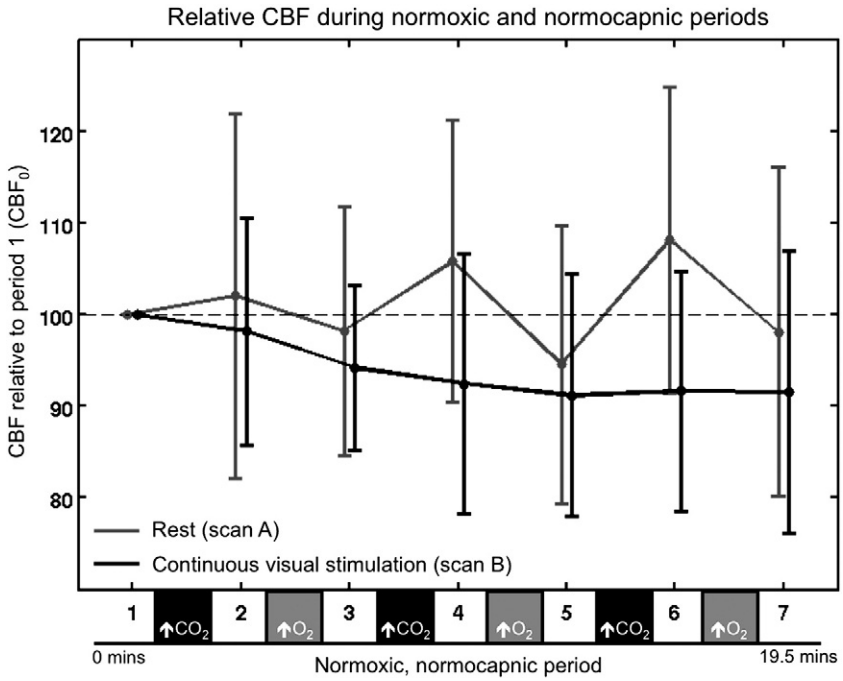

Fig. 5. Long-term trend of CBF within the visual region of interest. We show the CBF during the normocapnic, normoxic periods relative to the first such period of scans A (rest) and B (continuous reversing checkerboard). CBF is plotted for the region of interest in visual cortex defined as active from the visual stimulus applied in scan C. Error-bars indicate the standard deviation in relative CBF across the cohort of 11 subjects. Seven periods of CBF are plotted. There was a significant downward trend in the CBF during continuous visual stimulation compared to the resting scan.

and hypercapnia protocol, in which α and β were also estimated, yielded lower global grey matter $CMRO_2$ values (156–185 μmol/100 g/min) depending on the combination of α and β used (Table 1), than the interleaved protocol (206–222 μmol/100 g/min), this being generally the case also on a regional basis (Table 2). The (0.91, 0.14) combination of (α, β) (Griffeth and Buxton, 2011) tended to yield lower $CMRO_2$ values than other combinations tested: (0.38, 1.5), (0.2, 1.3) and (0.18, 1.5). For the interleaved protocol, incorporating information on α and β from scan D, the combined protocol, reduced the $CMRO_2$ values towards those obtained in the combined protocol (Table 1) and towards those reported previously for PET. The recent MRI studies of Gauthier and Hoge (2012) and Bulte et al. (2012) reported group mean grey matter $CMRO_2$ values of 145 ± 30 and 155 ±39 μmol/100 g/min respectively.

Recently other MRI methods, not requiring the use of respiratory challenges, have been demonstrated that aim to measure OEF and absolute $CMRO_2$. Global $CMRO_2$ has been estimated through assessment of sagittal sinus oxygenation, yielding a value of 132 ± 20 μmol/100 g/min (Xu et al., 2009). However, this pools white matter and grey matter together. Under the assumption that $CMRO_2$ in white matter is half that in grey matter (Leenders et al., 1990) and that there is twice as much grey matter as white matter (Lüders et al., 2002), the study of Xu et al. (2009) would suggest a grey matter $CMRO_2$ of 158 μmol/100 g/min. Regional venous oxygenation measurements based on the phase of the MR signal have yielded grey matter $CMRO_2$ of 158 ± 18 μmol/100 g/min (Fan et al., 2012), although the spatial resolution of this method depends on identifying veins of suitable geometry. Methods with the potential for mapping on a voxel-wise basis OEF and $CMRO_2$ include velocity selective spin labelling (Bolar et al., 2011) (cortical grey matter $CMRO_2$ measured at 125 ± 15 and OEF 0.26 ± 0.02); velocity selective excitation and arterial nulling (Guo and Wong, 2012) (grey matter OEF estimated at 0.395 ± 0.025) and quantitative BOLD methods (He and Yablonskiy, 2007) (grey and white matter OEF = 0.38 ± 0.05).

The spatial distribution of $CMRO_2$ across the cortex mapped using our combined hyperoxia and hypercapnia protocol appears non-uniform (Table 2 and Fig. 4) with higher values in insula and occipital cortex where CBF was measured to be higher. This spatial variation, and in particular the higher values in those regions, is consistent with observations from ^{15}O PET studies (Ibaraki et al., 2010; Leenders et al., 1990). In occipital regions local values measured with PET at rest have been shown to exceed 200 μmol/100 g/min (Ibaraki et al., 2010). Again, consistent with PET, the OEF appears to be rather spatially uniform and the main determinant of the spatial variation of $CMRO_2$ appears to be the spatial variation of CBF.

Considering $CMRO_2$ as the product of CBF, the total arterial oxygen content and OEF (Eq. (5)), what are the potential systematic errors in the measurement of these quantities that may influence estimates of $CMRO_2$? Our estimates of global grey matter CBF lie around 56 ml/100 g/min, similar to those of Gauthier and Hoge (2012) (52 ml/100 g/min) but larger than those of Bulte et al. (2012) (41 ml/100 g/min) and those of Petersen et al. reported in a multi-centre ASL study (Petersen et al., 2010) (47 ml/100 g/min). Our CBF values are also larger than those measured by ^{15}O PET, for example, 46 ml/100 g/min (Ito et al., 2004) (cohort, 52 ± 15 years), 42 ml/100 g/ml (Ibaraki et al., 2010) (cohort 50–67 years) and 40–50 ml/100 g/min (Leenders et al., 1990). However, our values lie close to those of the younger group reported by Ances et al. (2009) (63 ml/100 g/min) obtained with a similar ASL acquisition scheme. Caution is urged in comparing CBF measurements as CBF will depend on the age distribution of the cohort, the cortical regions examined and the degree of partial volume present in the region of interest of grey and white matter, CBF being lower in white matter. Our higher estimates of regional CBF than some of those previously reported may arise from the specific ASL acquisition adopted and signal model assumed. We used a pulsed ASL approach with a single post-labelling delay. Greater confidence in CBF quantitation may be obtained with multiple post-labelling delays (Gallichan and Jezzard, 2009), although with a likely penalty in acquisition time. A pCASL approach could also be used with multiple post-labelling delays, and which may offer enhanced perfusion

contrast-to-noise. However, pCASL suffers the disadvantage of velocity-dependent labelling which could bias the measurement of CBF responses to hypercapnia (Aslan et al., 2010; Bulte et al., 2012). We have estimated the carriage of oxygen in arterial blood from the measured end-tidal partial pressure of oxygen, without correcting for the alveolar–arterial gradient of oxygen. This gradient being small (5–10 mm Hg) it has little effect on the calculated arterial oxygen content (Bulte et al., 2012). Our estimates of OEF are larger than those of Bulte et al. (2012) (0.38) and Gauthier and Hoge (2012) (0.35), and are dependent on the assumed values of α and β or whether they were estimated from the data. For global grey matter our OEF estimates lay in the range 0.37–0.50 for the interleaved protocol and 0.36–0.42 for the combined protocol, these ranges being closer to those reported in PET studies ((Leenders et al., 1990) typically 0.40–0.43, (Ito et al., 2004) 0.44 ± 0.06 and (Ibaraki et al., 2010) 0.42–0.45), than the studies of Bulte et al. (2012) and Gauthier and Hoge (2012), although between-subject variation suggests that larger cohorts are needed for more definitive comparisons.

Estimates of α, the constant exponent relating relative changes in CBV to CBF, and β, the constant linking blood oxygenation to signal relaxation (Boxerman et al., 1995) were made on a regional and on a voxel-wise basis. Over all grey matter α was estimated to be 0.33 ± 0.06 and $\beta = 1.35 \pm 0.13$. This estimate of β at 3 T lies below the commonly applied $\beta = 1.5$, which is likely to be more appropriate for a field strength of 1.5 T given the expectation of reduced β with higher field strength (Buxton, 2002). The spatial variation of α and β is not marked (Fig. 4 and Table 2). Values of α have been reported previously and depend on the balance of blood volume compartments, arterial or venous, from which measurements are made. Estimates from total blood volume in anaesthetised monkeys undergoing a global CO_2 challenge have given $\alpha = 0.38$ (Grubb et al., 1974), until now, the most commonly applied value in calibrated fMRI. However, traditional BOLD fMRI is normally most sensitive to venous blood volume under normal physiological conditions. Focussing on venous volume, recent studies have yielded values of α lower than 0.38, for example $\alpha = 0.18 \pm 0.02$ (Chen and Pike, 2010b); and $\alpha = 0.16 \pm 0.02$ (Mark and Pike, 2012) with higher and lower values in different cortical regions and $\alpha = 0.14$ has been estimated from detailed modelling studies (Griffeth and Buxton, 2011). Our observed BOLD signal changes are likely to be dominated by venous blood. However, our estimate of α may be closer to that of Grubb et al. (1974) than recent fMRI-based studies because of potential hyperoxia-induced BOLD contribution from the arterial side of the vasculature, where oxygen saturation is not quite 100% during normoxia (Schwarzbauer and Deichmann, 2012).

The simultaneous administration of hyperoxia and hypercapnia allowed α and β to be estimated, the changes in arterial oxygen content offering a CBV dependent signal (Blockley et al., 2012a; Driver et al., 2012) as CBF is altered through hypercapnia. It was not possible to estimate these parameters from the interleaved protocol. Even with the combined graded hypercapnia and hyperoxia protocol we need to be aware of the fact that there is likely to be a degree of colinearity between α and β. This is apparent from Eq. (6) giving the ratio of hyperoxia-induced BOLD signal changes at different levels of CBF, where the dependence reduced to a single exponent ($\eta = (1+\alpha-\beta)$). Indeed, that exponent was used to constrain the fitting of data from the interleaved protocol (Table 1). However, considering the full signal changes, rather than ratios, Eqs. (4) and (1) suggest some separability of α and β. Further detailed signal modelling studies such as explored by Griffeth and Buxton (2011) would be valuable in quantifying and optimising this separability further under a range of oxygenation and flow levels.

The fractional increase in $CMRO_2$ arising from the 90 s visual task was estimated to be 16 or 18% (Table 4) depending on the chosen values of α and β. By comparison, the fractional increase appeared slightly smaller for the 20 min continuous visual task compared to rest: 13 or 11% depending on α and β. Whilst this discrepancy may arise from a bias introduced by the choice of region of interest, defined from the 90 s visual task, it may also be suggestive of a reduction of stimulus-induced increase in $CMRO_2$ over the long time course of the visual stimulus. This notion would be supported, in the event of a fixed metabolism:CBF coupling ratio, by the decline in CBF evident during the 20 min stimulus in Fig. 5. Towards the end of visual stimulation the CBF in visual cortex appears to fall by about 10% relative to that at the start, a decline that is not seen over the 20 min course of the scan at rest. This would be consistent with neuronal habituation during a long stimulus (Bandettini et al., 1997).

Our combined approach of intermittent hyperoxia with multiple levels of hypercapnia has the capacity to reduce the number of parameters that have to be assumed in the BOLD signal model. This expands the range of physiological and pathophysiological conditions in which it might be applied. For example, where vessel architecture is altered it may not be appropriate to assume a value for β, whilst in circumstances of altered vascular tone, perhaps in the ageing brain or with pharmacological intervention, measurement of α may be necessary as well as offering a potential marker of vascular health.

Our image acquisition used a dual-echo spiral acquisition to minimise R_2^* related signal loss in the first echo with a short echo-time of 3 ms and was used for CBF quantification whilst the later echo was used to maximise BOLD sensitivity. A dual-echo approach was also used in the same manner by Gauthier and Hoge (2012) but with a Cartesian EPI readout, whilst Bulte et al. (2012) used a single echo to obtain BOLD and CBF information. The present study did not compare spiral readout with Cartesian EPI, although the benefits of spiral acquisition have been discussed elsewhere (Glover, 2012).

The estimation of OEF relied on the non-linear model presented and therefore required a non-linear fitting approach. The number of fitted data points for each experimental run was relatively small, having been averaged into 44 s blocks before fitting. Conventional non-linear fitting routines are prone to the effects of outlier datapoints, leading to boundary-condition solutions which are not physiologically plausible. The Bayesian approach used here helps circumvent this problem by de-weighting the influence of outliers based on the Gaussian priors. The data from the combined approach was successfully fitted in more subjects than from the interleaved approach in the region of interest analysis (Table 1). In the voxel-wise mapping (Fig. 4) white matter was excluded due to a lack of perfusion weighted signal there, arising from the long arrival times of the inversion label. Different numbers of subjects contributed to the group average parameters displayed at different voxels as only those subjects whose data were successfully fitted were retained at each location (Fig. 4h). The success rates in terms of a number of subjects successfully fitted, for all regions of interest (baseline or task) and all parts of the experiment are quoted in Tables 1–3. For baseline $CMRO_2$, the reliability in achieving an estimate lay at typically 80–90%, although ranged from 64 to 100% depending on the region of interest and experimental method used.

The combined design has the advantage of a shorter acquisition time (13 min for the combined but 19.5 min for the interleaved approach) and therefore represents a more efficient approach to data collection. The interleaved approach can be conducted without a complex end-tidal forcing system (Wise et al., 2007) or prospective end-tidal targeting system (Slessarev et al., 2007) but instead can be performed using a fixed inspired challenge (Bulte et al., 2012) with manual control of gas flows. However, for the combined approach it is likely to be difficult to achieve sufficient stable periods of end-tidal levels with manual control of gases. Predictive and feedback based control of end-tidal gases also has the advantage of faster transitions (Wise et al., 2007), reducing the time taken for data acquisition. This is especially valuable in the transition from hyperoxia to normoxia where the introduction of a mildly hypoxic inspirate forces down the arterial oxygen tension faster than if normal air is administered. Without this, a period of a couple of minutes, at least, is needed

to return to normoxia (Bulte et al., 2012). Our approach to data analysis, in which we averaged blocks of data to improve signal to noise, was facilitated by the stability of gas levels offered by end-tidal forcing. However, neither clamping of one gas tension to baseline levels whilst the other is changed nor avoidance of dynamic changes in O_2 and CO_2 levels likely to occur during manual control of gas flows would be a strict requirement for success of the proposed combined approach as the BOLD signal model is formulated to accommodate simultaneous changes in both CO_2 and O_2.

The methods described do require the participant to wear a face-mask in the scanner for the supply of altered concentrations of inspired gases. Whilst we did not formally canvass descriptions of the sensations experienced by the volunteers, some volunteers notice the level of hypercapnia that we induced as a mild air-hunger accompanied by an increased breathing rate, akin to the effects of physical exercise. This effect subsides within a few seconds with restoration of normocapnia. Hyperoxia was imperceptible. Some patient groups may find the measurement procedure difficult, for example, those with respiratory disorders, in which end-tidal measurements may also be unrepresentative of arterial blood gas levels, or individuals who suffer from claustrophobia, as the wearing of a face-mask in the scanner may potentiate feelings of confinement.

The BOLD signal model that we have chosen to apply is a simplification of the underlying biophysical phenomena as recently described (Blockley et al., 2012b; Griffeth and Buxton, 2011; Pike, 2011). However, modelling has shown that it offers in many circumstances a reasonable description of the experimental data in particular because the parameters α and β offer enough flexibility to account for explicitly un-modelled phenomena such as intravascular BOLD (the model assumes that extravascular BOLD dominates), the small BOLD contribution from the arterial side of the vasculature, the paramagnetic effect of additional dissolved oxygen and variations in vessel size (Griffeth and Buxton, 2011; Schwarzbauer and Deichmann, 2012). In any of the methods that employ hypercapnia for BOLD signal calibration there is the potential for systematic error if hypercapnia modulates resting $CMRO_2$. The isometabolic nature of mild hypercapnia has been a topic of recent debate in the literature with Xu et al. (2011) finding a 13.4% reduction in $CMRO_2$ with 5% inspired CO_2, whilst Chen and Pike (2010a) found no significant alterations when both end-tidal CO_2 and O_2 were carefully controlled. However, Bulte et al. (2012) estimate that likely modulations in $CMRO_2$, should they exist, have a minor effect on the estimated OEF. Unlike Bulte et al. (2012) we have not used the hyperoxia related signal changes to estimate CBV, those calculations relying on an intravascular tracer (Bulte et al., 2007a) whereas most of the BOLD contrast arising in hyperoxia at 3 T is extravascular (Blockley et al., 2013; Lu and Van Zijl, 2005). A further subtle effect of hyperoxia is a reduction in CBF through a combination of vasoconstriction and lowering of arterial carbon dioxide tension (Floyd et al., 2003). The hypocapnic vasoconstriction can be mitigated as in the present study and as demonstrated by Mark et al. (2011), through the maintenance of isocapnia using end-tidal forcing. The residual vasoconstrictive effects of hyperoxia (Bulte et al., 2007b), small at our chosen levels of hyperoxia, are accounted for by our measurement of CBF and its inclusion in the BOLD signal model.

In this study, we have demonstrated a method of measuring absolute $CMRO_2$ (along with other relevant biophysical parameters: M, SvO_2, α and β) using respiratory-based BOLD calibration methods. We have further demonstrated the ability to measure within-subject changes in absolute $CMRO_2$. The advantages of using this approach to measure absolute $CMRO_2$ compared to PET lie in the avoidance of a radioactive tracer. This opens the possibility of serial scans in healthy volunteers and patients permitting study of brain development, brain plasticity and ageing as well as disease monitoring and longitudinal assessment of treatments. In a similar manner to the recent MR founded resurgence in mapping CBF to characterise chronic conditions such as pain (Howard et al., 2011), we anticipate that the ability to map across the brain absolute $CMRO_2$ will offer a valuable probe to characterise neurological and psychiatric disease.

Acknowledgments

RW thanks the Higher Education Funding Council for Wales and the UK Engineering and Physical Sciences Research Council (reference EP/K020404/1). AH is funded by the Banting Fellowship Program, NSERC of Canada. AS is supported by a Cardiff University President's Research Scholarship. KM is funded by a Wellcome Trust Career Development Award. The authors thank Dr. Tom Liu of the Center for fMRI at University of California San Diego with help in setting up the imaging sequences.

Appendix A

We aim to develop the model of the BOLD signal to describe the effects of CBF changes brought about by changes in the partial pressure of arterial CO_2 ($PaCO_2$) and increases in the partial pressure of arterial O_2 (PaO_2) only. We begin from the model of Davis et al. (1998) and Hoge et al. (1999b), describing fractional BOLD signal changes ($\Delta S/S_0$) in terms of CBV and venous deoxyhaemoglobin concentration [dHb] in which the subscript '0' indicates the baseline (normoxic and normocapnic) conditions:

$$\frac{\Delta S}{S_0} = M\left\{1-\left(\frac{CBF}{CBF_0}\right)^{\alpha}\left(\frac{[dHb]}{[dHb]_0}\right)^{\beta}\right\} \tag{A1}$$

in which the power law substitution relating fractional changes in blood flow and blood volume has been made,

$$\left(\frac{CBV}{CBV_0}\right) = \left(\frac{CBF}{CBF_0}\right)^{\alpha}. \tag{A2}$$

M is the maximum possible BOLD signal change and is given by:

$$M = TE\cdot A\cdot CBV_0\cdot[dHb]_0^{\beta} \tag{A3}$$

A and β are constants that depend on vessel size and geometry as well as magnetic field strength.

We aim to find an expression for $([dHb]/[dHb]_0)$. According to the conservation of mass (Fick's principle) the cerebral rate of consumption is given by:

$$CMRO_2 = (CaO_2 - CvO_2)\cdot CBF \tag{A4}$$

where CaO_2 and CvO_2 are the arterial and venous oxygen contents respectively and CBF represents blood flow to the tissue bed in which oxygen is extracted.

We assume that $CMRO_2$ is unaltered during hypercapnic and hyperoxic challenges compared to the baseline condition, therefore:

$$\left(CaO_2|_0 - CvO_2|_0\right)\cdot CBF_0 = (CaO_2 - CvO_2)\cdot CBF. \tag{A5}$$

The venous oxygen content can be calculated from that bound to haemoglobin and that dissolved in the plasma:

$$CvO_2 = \phi[Hb]SvO_2 + PvO_2\cdot\varepsilon \tag{A6}$$

where SvO_2 is the venous blood oxygen saturation, ε is the coefficient of solubility of oxygen in blood (0.0031 ml O_2/(dl_{blood} mm Hg)) and ϕ is the O_2 carrying capacity of haemoglobin (1.34 ml O_2/g_{Hb}). In practice, the dissolved oxygen ($PvO_2\cdot\varepsilon$) is negligible in venous plasma. We assume the concentration of haemoglobin to be [Hb] = 15 g Hb $dl^{-1}{}_{blood}$.

Substituting A6 into A5:

$$\frac{CBF_0}{CBF} = \frac{CaO_2 - (\phi[Hb]SvO_2)}{CaO_2|_0 - (\phi[Hb]SvO_2|_0)} \tag{A7}$$

and the venous deoxyhaemoglobin concentration is given by

$$[dHb] = [Hb](1 - SvO_2). \tag{A8}$$

Substituting A8 into A7 gives:

$$\frac{CBF_0}{CBF} = \frac{CaO_2 - \phi([Hb] - [dHb])}{CaO_2|_0 - \phi([Hb] - [dHb]_0)}. \tag{A9}$$

Rearranging A9 gives an expression for venous deoxyhaemoglobin concentration with respect to baseline (normoxia and normocapnia) when arterial oxygen content is increased and/or CBF is altered:

$$\frac{[dHb]}{[dHb]_0} = \frac{CBF_0}{CBF} - \frac{1}{[dHb]_0}\left\{\frac{1}{\phi}\left(CaO_2 - \left(\frac{CBF_0}{CBF}\right)CaO_2|_0\right) + [Hb]\left(\frac{CBF_0}{CBF} - 1\right)\right\} \tag{A10}$$

for which the arterial oxygen content,

$$CaO_2 = \phi[Hb]SaO_2 + PaO_2 \cdot \varepsilon, \tag{A11}$$

can be calculated using the relationship between oxygen partial pressure (PaO_2) and arterial oxygen saturation (SaO_2), (the Severinghaus equation):

$$SaO_2 = \left(\frac{1}{\frac{23400}{(PaO_2)^3 + 150(PaO_2)} + 1}\right). \tag{A12}$$

We substitute Eq. (A10) into Eq. (A1) and fit for M and $SvO_2|_0$ where $[dHb]_0 = [Hb](1 - SvO_2|_0)$. Baseline rate of cerebral oxygen consumption is given (in ml O_2/100 g/min) by:

$$CMRO_2|_0 = (CaO_2|_0 - CvO_2|_0) \cdot CBF_0 = CaO_2|_0 \cdot OEF_0 \cdot CBF_0. \tag{A13}$$

allowing OEF_0 also to be calculated once $SvO_2|_0$ is estimated.

Together Eqs. (A10) and (A1) characterise the BOLD signal and incorporate the parameters α and β. Experimental data acquired with simultaneous modulation of CBF and arterial oxygen content allowed α and β to be estimated from the full signal model (Eqs. (A10) and (A1)) in addition to M and $SvO_2|_0$ and therefore $CMRO_2|_0$ and OEF_0.

In the specific case of increased arterial oxygen content on top of increased CBF induced by hypercapnia we can formulate a relationship, based on the ratio of oxygen related BOLD signal changes at different levels of CBF, which can be used to constrain estimates of α and β in combination with data acquired from interleaved hypercapnia and hyperoxia.

We begin with the expression Eq. (A1) for the ith level of hypercapnia,

$$\frac{\Delta S_i}{S_i} = TE \cdot A \cdot CBV_i \cdot [dHb_i]_0^{\beta}\left\{1 - \left(\frac{CBF_i}{CBF_i|_0}\right)^{\alpha}\left(\frac{[dHb_i]}{[dHb_i]_0}\right)^{\beta}\right\} \tag{A14}$$

considering $i = 1$ for one level of hypercapnia e.g. normocapnia and $i = 2$ for a different level of hypercapnia. The ratio of oxygen-related signal changes where there is no CBF change with hyperoxia is given by:

$$\frac{\Delta S_1}{\Delta S_2}\frac{S_2}{S_1} = \frac{CBV_1}{CBV_2} \cdot \frac{[dHb_1]_0^{\beta}}{[dHb_2]_0^{\beta}}\left\{\frac{1 - \left(\frac{[dHb_1]}{[dHb_1]_0}\right)^{\beta}}{1 - \left(\frac{[dHb_2]}{[dHb_2]_0}\right)^{\beta}}\right\} \tag{A15}$$

where $[dHb_i]_0$ and $[dHb_i]$ represent deoxyhaemoglobin concentrations for the ith level of hypercapnia at baseline and elevated PaO_2.

We can expand the ratio of deoxyhaemoglobin concentrations with a binomial series assuming that the arterial hyperoxia related change in [dHb] is small, namely $\left(\frac{[dHb] - [dHb]_0}{[dHb]_0}\right) << 1$.

$$\frac{[dHb_i]^{\beta}}{[dHb_i]_0} = \left(1 + \frac{[dHb_i] - [dHb_i]_0}{[dHb_i]_0}\right)^{\beta} = 1 + \beta\left(\frac{[dHb_i] - [dHb_i]_0}{[dHb_i]_0}\right) + \ldots$$

Substituting the first two terms into Eq. (A16)

$$\frac{\Delta S_1}{\Delta S_2}\frac{S_2}{S_1} = \frac{CBV_1}{CBV_2} \cdot \frac{[dHb_1]^{\beta-1}}{[dHb_2]^{\beta-1}}\left\{\frac{[dHb_1] - [dHb_1]_0}{[dHb_2] - [dHb_2]_0}\right\}. \tag{A16}$$

Then assuming that the hyperoxia related changes in BOLD signal are small, namely $S_1 \cong S_2$ and for a pure change in CBF, $\frac{[dHb_1]_0}{[dHb_2]_0} \cong \frac{CBF_2}{CBF_1}$, then

$$\frac{\Delta S_1}{\Delta S_2} = \left(\frac{CBF_1}{CBF_2}\right)^{\alpha} \cdot \frac{(CBF_2)^{\beta-1}}{(CBF_1)^{\beta-1}}\left\{\frac{[dHb_1] - [dHb_1]_0}{[dHb_2] - [dHb_2]_0}\right\}. \tag{A17}$$

During experimentation, $[dHb_i] - [dHb_i]_0$ is not directly measured. However, for an increase in arterial oxygen content during hyperoxia, under the assumption that oxygen metabolism is unchanged, the extraarterial oxygen appears as a change in venous deoxyhaemoglobin concentration. Namely, $[dHb_i] - [dHb_i]_0$ is proportional to $\Delta CaO_2|_i = CaO_2|_{i,hyperoxia} - CaO_2|_{i,normoxia}$, the difference in arterial oxygen content induced by hyperoxia at the ith level of CBF. Therefore,

$$\frac{\Delta S_{1,O_2}}{\Delta S_{2,O_2}} = \left(\frac{CBF_1}{CBF_2}\right)^{1+\alpha-\beta} \tag{A18}$$

where $\Delta S_{i,O_2} = \frac{\Delta S_i}{\Delta CaO_2|_i}$ is the hyperoxia-induced BOLD signal change normalized to the hyperoxia-induced change in total arterial oxygen content, administered at the ith hypercapnic (CBF) level. This gives us a relationship which we can use with the experimental data from combined hypercapnia and hyperoxia to estimate $(1+\alpha-\beta)$.

Conflict of interest

The authors have no conflicts of interest to declare in respect of the content of this article.

References

Ances, B.M., Liang, C.L., Leontiev, O., Perthen, J.E., Fleisher, A.S., Lansing, A.E., Buxton, R.B., 2009. Effects of aging on cerebral blood flow, oxygen metabolism, and blood oxygenation level dependent responses to visual stimulation. Hum. Brain Mapp. 30, 1120–1132.

Aslan, S., Xu, F., Wang, P.L., Uh, J., Yezhuvath, U.S., Van Osch, M., Lu, H., 2010. Estimation of labeling efficiency in pseudocontinuous arterial spin labeling. Magn. Reson. Med. 63, 765–771.

Bandettini, P.A., Kwong, K.K., Davis, T.L., Tootell, R.B., Wong, E.C., Fox, P.T., Belliveau, J.W., Weisskoff, R.M., Rosen, B.R., 1997. Characterization of cerebral blood oxygenation and flow changes during prolonged brain activation. Hum. Brain Mapp. 5, 93–109.

Blockley, N.P., Driver, I.D., Fisher, J. a, Francis, S.T., Gowland, P. a, 2012a. Measuring venous blood volume changes during activation using hyperoxia. NeuroImage 59, 3266–3274.

Blockley, N.P., Griffeth, V.E.M., Buxton, R.B., 2012b. A general analysis of calibrated BOLD methodology for measuring $CMRO_2$ responses: comparison of a new approach with existing methods. NeuroImage 60, 279–289.

Blockley, N.P., Griffeth, V.E.M., Germuska, M. a, Bulte, D.P., Buxton, R.B., 2013. An analysis of the use of hyperoxia for measuring venous cerebral blood volume: comparison of the existing method with a new analysis approach. NeuroImage 72, 33–40.

Bolar, D.S., Rosen, B.R., Sorensen, A.G., Adalsteinsson, E., 2011. Quantitative imaging of extraction of oxygen and tissue consumption (QUIXOTIC) using venular-targeted velocity-selective spin labeling. Magn. Reson. Med. 66, 1550–1562.

Boxerman, J.L., Bandettini, P. a, Kwong, K.K., Baker, J.R., Davis, T.L., Rosen, B.R., Weisskoff, R.M., 1995. The intravascular contribution to fMRI signal change:

Monte Carlo modeling and diffusion-weighted studies in vivo. Magn. Reson. Med. 34, 4–10.
Bulte, D., Chiarelli, P., Wise, R., Jezzard, P., 2007a. Measurement of cerebral blood volume in humans using hyperoxic MRI contrast. J. Magn. Reson. Imaging 26, 894–899.
Bulte, D.P., Chiarelli, P. a, Wise, R.G., Jezzard, P., 2007b. Cerebral perfusion response to hyperoxia. J. Cereb. Blood Flow Metab. 27, 69–75.
Bulte, D.P., Kelly, M., Germuska, M., Xie, J., Chappell, M. a, Okell, T.W., Bright, M.G., Jezzard, P., 2012. Quantitative measurement of cerebral physiology using respiratory-calibrated MRI. NeuroImage 60, 582–591.
Buxton, R.B., 2002. An Introduction to Functional Magnetic Resonance Imaging: Principles and Techniques, First ed. Cambridge University Press, Cambridge.
Chen, J.J., Pike, G.B., 2010a. Global cerebral oxidative metabolism during hypercapnia and hypocapnia in humans: implications for BOLD fMRI. J. Cereb. Blood Flow Metab. 30, 1094–1099.
Chen, J.J., Pike, G.B., 2010b. MRI measurement of the BOLD-specific flow-volume relationship during hypercapnia and hypocapnia in humans. NeuroImage 53, 383–391.
Chiarelli, P.A., Bulte, D.P., Wise, R., Gallichan, D., Jezzard, P., 2007. A calibration method for quantitative BOLD fMRI based on hyperoxia. NeuroImage 37, 808–820.
Davis, T.L., Kwong, K.K., Weisskoff, R.M., Rosen, B.R., 1998. Calibrated functional MRI: mapping the dynamics of oxidative metabolism. Proc. Natl. Acad. Sci. U. S. A. 95, 1834–1839.
Driver, I.D., Hall, E.L., Wharton, S.J., Pritchard, S.E., Francis, S.T., Gowland, P. a, 2012. Calibrated BOLD using direct measurement of changes in venous oxygenation. NeuroImage 63, 1178–1187.
Fan, A.P., Benner, T., Bolar, D.S., Rosen, B.R., Adalsteinsson, E., 2012. Phase-based regional oxygen metabolism (PROM) using MRI. Magn. Reson. Med. 67, 669–678.
Floyd, T.F., Clark, J.M., Gelfand, R., Detre, J. a, Ratcliffe, S., Guvakov, D., Lambertsen, C.J., Eckenhoff, R.G., 2003. Independent cerebral vasoconstrictive effects of hyperoxia and accompanying arterial hypocapnia at 1 ATA. J. Appl. Physiol. 95, 2453–2461.
Gallichan, D., Jezzard, P., 2009. Variation in the shape of pulsed arterial spin labeling kinetic curves across the healthy human brain and its implications for CBF quantification. Magn. Reson. Med. 61, 686–695.
Gauthier, C.J., Hoge, R.D., 2012. Magnetic resonance imaging of resting OEF and CMRO using a generalized calibration model for hypercapnia and hyperoxia. NeuroImage 60, 1212–1225.
Glover, G.H., 1999. Simple analytic spiral K-space algorithm. Magn. Reson. Med. 42, 412–415.
Glover, G.H., 2012. Spiral imaging in fMRI. NeuroImage 62, 706–712.
Glover, G.H., Li, T.Q., Ress, D., 2000. Image-based method for retrospective correction of physiological motion effects in fMRI: RETROICOR. Magn. Reson. Med. 44, 162–167.
Griffeth, V.E.M., Buxton, R.B., 2011. A theoretical framework for estimating cerebral oxygen metabolism changes using the calibrated-BOLD method: modeling the effects of blood volume distribution, hematocrit, oxygen extraction fraction, and tissue signal properties on the BOLD signal. NeuroImage 58, 198–212.
Grubb Jr., R.L., Raichle, M.E., Eichling, J.O., Ter-Pogossian, M.M., 1974. The effects of changes in $PaCO_2$ on cerebral blood volume, blood flow, and vascular mean transit time. Stroke 5, 630–639.
Guo, J., Wong, E.C., 2012. Venous oxygenation mapping using velocity-selective excitation and arterial nulling. Magn. Reson. Med. 68, 1458–1471.
Harvey, A.K., Pattinson, K.T., Brooks, J.C., Mayhew, S.D., Jenkinson, M., Wise, R.G., 2008. Brainstem functional magnetic resonance imaging: disentangling signal from physiological noise. J. Magn. Reson. Imaging 28, 1337–1344.
He, X., Yablonskiy, D.A., 2007. Quantitative BOLD: mapping of human cerebral deoxygenated blood volume and oxygen extraction fraction: default state. Magn. Reson. Med. 57, 115–126.
He, X., Zhu, M., Yablonskiy, D.A., 2008. Validation of oxygen extraction fraction measurement by qBOLD technique. Magn. Reson. Med. 60, 882–888.
Hoge, R.D., Atkinson, J., Gill, B., Crelier, G.R., Marrett, S., Pike, G.B., 1999a. Linear coupling between cerebral blood flow and oxygen consumption in activated human cortex. Proc. Natl. Acad. Sci. U. S. A. 96, 9403–9408.
Hoge, R.D., Atkinson, J., Gill, B., Crelier, G.R., Marrett, S., Pike, G.B., 1999b. Investigation of BOLD signal dependence on cerebral blood flow and oxygen consumption: the deoxyhemoglobin dilution model. Magn. Reson. Med. 42, 849–863.
Howard, M.A., Krause, K., Khawaja, N., Massat, N., Zelaya, F., Huggins, J.P., Vennart, W., Williams, S.C.R., Renton, T.F., 2011. Beyond patient reported pain: perfusion magnetic resonance imaging demonstrates reproducible cerebral representation of ongoing post-surgical pain. PLoS One 6, e17096.
Iannetti, G.D., Wise, R.G., 2007. BOLD functional MRI in disease and pharmacological studies: room for improvement? Magn. Reson. Imaging 25, 978–988.
Ibaraki, M., Shinohara, Y., Nakamura, K., Miura, S., Kinoshita, F., Kinoshita, T., 2010. Interindividual variations of cerebral blood flow, oxygen delivery, and metabolism in relation to hemoglobin concentration measured by positron emission tomography in humans. J. Cereb. Blood Flow Metab. 30, 1296–1305.
Ito, H., Kanno, I., Kato, C., Sasaki, T., Ishii, K., Ouchi, Y., Iida, A., Okazawa, H., Hayashida, K., Tsuyuguchi, N., Ishii, K., Kuwabara, Y., Senda, M., 2004. Database of normal human cerebral blood flow, cerebral blood volume, cerebral oxygen extraction fraction and cerebral metabolic rate of oxygen measured by positron emission tomography with 15O-labelled carbon dioxide or water, carbon monoxide and oxygen. Eur. J. Nucl. Med. Mol. Imaging 31.
Jenkinson, M., Smith, S., 2001. A global optimisation method for robust affine registration of brain images. Med. Image Anal. 5, 143–156.
Jenkinson, M., Bannister, P., Brady, M., Smith, S., 2002. Improved optimization for the robust and accurate linear registration and motion correction of brain images. NeuroImage 17, 825–841.
Leenders, K.L., Perani, D., Lammertsma, a a, Heather, J.D., Buckingham, P., Healy, M.J., Gibbs, J.M., Wise, R.J., Hatazawa, J., Herold, S., 1990. Cerebral blood flow, blood volume and oxygen utilization. Normal values and effect of age. Brain 113, 27–47.
Liu, T.T., Wong, E.C., 2005. A signal processing model for arterial spin labeling functional MRI. NeuroImage 24, 207–215.
Liu, T.T., Wong, E.C., Frank, L.R., Buxton, R.B., 2002. Analysis and design of perfusion-based event-related fMRI experiments. NeuroImage 16, 269–282.
Lu, H., Ge, Y., 2008. Quantitative evaluation of oxygenation in venous vessels using T2-Relaxation-Under-Spin-Tagging MRI. Magn. Reson. Med. 60, 357–363.
Lu, H., Van Zijl, P.C.M., 2005. Experimental measurement of extravascular parenchymal BOLD effects and tissue oxygen extraction fractions using multi-echo VASO fMRI at 1.5 and 3.0 T. Magn. Reson. Med. 53, 808–816.
Lüders, E., Steinmetz, H., Jäncke, L., 2002. Brain size and grey matter volume in the healthy human brain. Neuroreport 13, 2371–2374.
Mark, C.I., Pike, G.B., 2012. Indication of BOLD-specific venous flow-volume changes from precisely controlled hyperoxic vs. hypercapnic calibration. J. Cereb. Blood Flow Metab. 32, 709–719.
Mark, C.I., Fisher, J.A., Pike, G.B., 2011. Improved fMRI calibration: precisely controlled hyperoxic versus hypercapnic stimuli. NeuroImage 54, 1102–1111.
Petersen, E.T., Mouridsen, K., Golay, X., 2010. The QUASAR reproducibility study, part II: results from a multi-center arterial spin labeling test–retest study. NeuroImage 49, 104–113.
Pike, G.B., 2011. NeuroImage quantitative functional MRI: concepts, issues and future challenges. NeuroImage 62, 1234–1240.
Schwarzbauer, C., Deichmann, R., 2012. Vascular component analysis of hyperoxic and hypercapnic BOLD contrast. NeuroImage 59, 2401–2412.
Slessarev, M., Han, J., Mardimae, A., Prisman, E., Preiss, D., Volgyesi, G., Ansel, C., Duffin, J., Fisher, J. a, 2007. Prospective targeting and control of end-tidal CO_2 and O_2 concentrations. J. Physiol. 581, 1207–1219.
Smith, S.M., 2002. Fast robust automated brain extraction. Hum. Brain Mapp. 17, 143–155.
Wise, R.G., Pattinson, K.T., Bulte, D.P., Chiarelli, P.A., Mayhew, S.D., Balanos, G.M., O'Connor, D.F., Pragnell, T.R., Robbins, P.A., Tracey, I., Jezzard, P., 2007. Dynamic forcing of end-tidal carbon dioxide and oxygen applied to functional magnetic resonance imaging. J. Cereb. Blood Flow Metab. 27, 1521–1532.
Wong, E.C., Buxton, R.B., Frank, L.R., 1998. Quantitative imaging of perfusion using a single subtraction (QUIPSS and QUIPSS II). Magn. Reson. Med. 39, 702–708.
Woolrich, M.W., Ripley, B.D., Brady, M., Smith, S.M., 2001. Temporal autocorrelation in univariate linear modeling of fMRI data. NeuroImage 14, 1370–1386.
Xu, F., Ge, Y., Lu, H., 2009. Noninvasive quantification of whole-brain cerebral metabolic rate of oxygen ($CMRO_2$) by MRI. Magn. Reson. Med. 62, 141–148.
Xu, F., Uh, J., Brier, M.R., Hart, J., Yezhuvath, U.S., Gu, H., Yang, Y., Lu, H., 2011. The influence of carbon dioxide on brain activity and metabolism in conscious humans. J. Cereb. Blood Flow Metab. 31, 58–67.